

Verification of 3 dimensional voids geometry in porous material with μ focus X-Ray CT - example of small glass ball aggregate -

Manabu TAKAHASHI⁽¹⁾, Haruka MINEMURA⁽²⁾ and Minoru SATO⁽²⁾

(1) National Institute of Advanced Industrial Science and Technology, Japan

E-mail:takahashi-gonsuke@aist.go.jp

(2) Tsukuba University

Abstract

Three dimensional geometry and connectivity of pore space play a fundamental role in governing fluid transport properties of ground materials. Small glass ball aggregate was selected as a standard porous materials representing a ground material. We analyzed three dimensional geometrical data of small glass ball aggregate obtained by micro focus X-ray CT. We introduced the three-dimensional medial axis (3DMA) method of Lindquist et al. (2000) to quantify the flow-relevant geometric properties of the voids structure in small glass ball aggregate. Using these data, we evaluated the number of total pore, interior pore, throat, coordination number, connecting path between two faces, tortuosity and the shortest path distribution within an arbitrary region. Various analyzed geometrical information are good in harmony with theoretical data in geometry of porous media. We also present the spatial distribution of void space in arbitrary volume set. We can confidently say that microstructural information on geo-materials will greatly advance if micro focus X-ray CT is used concurrently as a tool of data analysis.

Keywords: voids geometry, μ focus X-Ray CT, 3-Dimensional Medial Axis, small glass ball aggregate

1. Introduction

Physical properties in rock are depending strongly on existence of voids space in rock. Quantification of total porosity and pore size distribution in rock can be done with Mercury Intrusion Porosimetry, but geometrical and spatial information in voids space are not obtained. X-ray Computerized Tomography (CT) has become nowadays a common nondestructive tool in a variety field. Some recent advances of X-ray CT in rock material fields are reviewed by Vervoort et al. (2003). The following publications are for example.

1) Determination of open fractures;

Verhelst et al. (1995) observed fracture openings of natural or induced fractures using a medical CT.

2) Determination of porosity and pore structures;

Coles et al. (2002) used a medical and micro focus CT and determined porosity and pore size distribution in sandstone to calculate hydraulic conductivity values. Hidajat et al. (2002) used microfocus CT to develop 3D images of the porosity in sandstone. Karacan et al. (2003) investigated a local porosity change of pressurized limestone using an X-ray transparent triaxial vessel.

3) Determination of fluid flow;

Hirono et al. (2003) measured the three

dimensional fluid flow distributions during permeability testing in fault related rocks using a medical CT. They concluded that fault zone was characterized by independent particulate flow as deformation mechanism act as conduits for fluid flow, whereas cataclastic fault zone act as barriers.

The application of X-ray CT in the non-destructive testing system of the mechanical properties of geomaterials, such as deformation and failure, is reported by Otani and Obara (2003).

It is well known that X-Ray CT is a good visualization tool as non-destructive and non-contact examination. We have introduced micro focus X-ray CT with high resolution of 10 micron to visualize and measure the voids space in porous media, especially sedimentary rocks like sandstone. We have introduced the three-dimensional medial axis (3DMA) method to quantify the flow-relevant geometric properties of the voids structure in porous media using micro focus X-Ray CT data. The number of connecting path between two faces, tortuosity and the shortest path distribution within an arbitrary region of sandstone specimen were analyzed. Geometrical information on the number of connecting path in an arbitrary volume CT data shows reasonable correlation between permeability anisotropy observed by laboratory permeability test and mutually

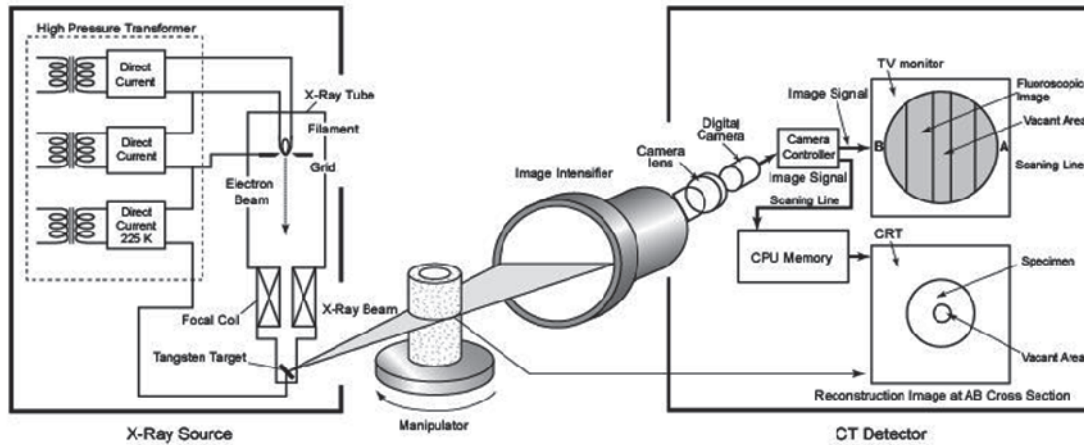


Fig.1 Schematic illustration of μ focus X-ray CT imaging system

perpendicular directions normal and parallel to bedding planes (Takahashi et al., 2014).

In this paper, we introduce geometrical information on voids connectivity, tortuosity distribution, shortest path distribution, and spatial distribution on a variety of voids size in aggregate of small glass ball.

2. CT system for micro focus X-Ray

Fig.1 shows the simplified structural layout of our micro focus X-ray CT apparatus comprising a source, CT imaging system, and CT detector. The internal structure of an object is determined according to the absorption rates of X-rays transmitted to the rotating object from many different angles. The system is able to reconstruct two-dimensional information of any cross-section, unlike the case for a fluoroscopic image, which presents information only for the X-ray projection. Micro focus X-ray CT is different from usual X-ray CT in that electron beams are narrowed before they reach the X-ray radiation source. A spatial resolution of $5 \mu\text{m}$ is attained by this additional function. The detector, which is usually coated with an image intensifier, acquires data through a digital camera. X-rays are converted into photoelectrons and/or visible light by the image intensifier. The analog signals are digitized by the digital camera and interpreted as the intensity of the transmitted X-rays incident to the image intensifier.

In this study, we used an X-ray CT system, HMX225, assembled by the TESCO Corporation (Fig. 2). The maximum voltage is 225kV, and focal spot size is 5 micro meter (Table 1). The so-called third generation CT system, which makes it possible to record X-ray attenuation at many angles by rotating an object on a computer-controlled rotation manipulator stage, is used in this instrument (Fig. 2).

Table 1 Specification in the TESCO Corporation HMX225

| Composition | Element | Specification |
|-------------------------------|---------------------------|---|
| X-Ray equipment (X-TEK 225MF) | Voltage / Focal spot size | 225kV / $5 \mu\text{m}$ |
| | Manipulator (M130-150) | Max weight / Diameter, Height 3Kg / 130, 150mm Max |
| X-ray Image system | Camera | High resolution CCD (12bit) |
| | Image intensifier | Input window $150\text{mm}\phi$ |
| CT equipment (BIR ACTIS+3) | Scan type | Offset / 180° / 360° / 3 slices |
| | Reconstruction time | 30 sec. |
| | Data output | TIFF, CAD |



Fig.2 Micro focus X-ray system assembled by TESCO Corporation

Attenuation data is detected by a 12bit CCD camera, and the recorded attenuation data are analyzed to reconstruct two-dimensionally an internal attenuation image of an object by means of a numerical technique known as filtered back projection. The resolution of 2D images is 1024×1024 pixels in this system. To obtain a clear boundary image between substances

having different attenuation coefficients, X-ray source must be small enough to minimize scattering zones on an X-ray detector, image intensifier

3. Definition of three dimensional medial axis analysis and example of glass beads packing

Lindquist and Venkatarangen (1999) developed the 3DMA computational package as a tool for analyzing the geometry of the pore and grain phases in three-dimensional CT data. Using this package, we can obtain the spatial distributions for pore and throat sizes, coordination number, tortuosity, and other geometrical relations between pores and throats.

In general, CT images of porous media are grayscale images and have a bimodal population, one mode corresponding to the signal from the pore space and the second to the signal from the grain space. As we are interested in the pore structure, an appropriate segmentation procedure is required to quantify the geometry of the pore space. The most suitable threshold procedure is selected to match a predetermined bulk density and porosity of the porous medium. In the 3DMA package, the kriging-based algorithm is used to segment the voxel images. The medial axis for a sphere is a straight line passing through the center point, and that for a cylinder is the axis of rotational symmetry. The medial axis for any n-dimensional object can be found by an algorithm equivalent to a “burning algorithm” (see Lindquist et al., 1996). Fig. 3 is a two-dimensional illustration of medial axis behavior for two nodal pores. A throat is defined as a local minimum of the cross sectional area in a channel.

For an object in a spatial continuum, the medial axis is a network of paths and vertices unless the object contains embedded cavities, where the medial axis also contains surface segments. For digitized objects, the medial axis consists of digitized paths corresponding to a connected line of voxels, digitized vertices corresponding to a cluster of one or more voxels, and possibly digitized surfaces corresponding

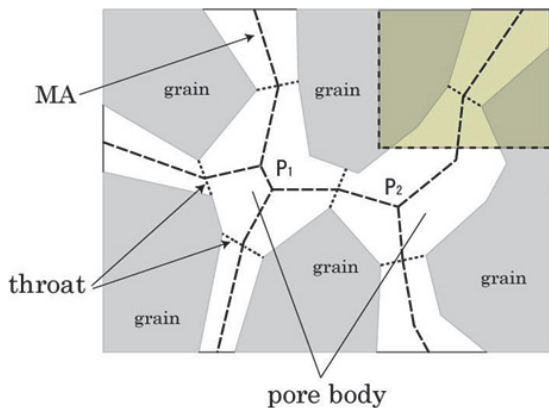


Fig. 3 Two Dimensional illustration of Medial Axis behavior

to a sheet of voxels. The usual conceptual model divides the void space of a porous medium into nodal pores connected by pore channels. Nodal pores are located at multigrain junctions. Roughly equidimensional in geometry, these nodal pores are joined to one another by pore channels, which include micro cracks situated along interfaces between two neighboring grains and tubular pores along three-grain edges.

Fig. 4 shows the original CT data and an example of medial axis analysis for the packing of glass beads with 600 μm diameters. We can visually confirm the accuracy of the medial axis analysis. The medial axis is affected by the flow channel, percolating backbone, and flow path in addition to other factors.

4. Verification of total porosity in glass ball packing

In a basis of mechanical behavior in granular material, the geometry of sphere packing is defined theoretically as Table 2. To confirm applicability of 3DMA method to quartz grain aggregate, we have measured pore geometry of small glass ball packing with various diameters. Fig. 4 shows the original CT data and an example of medial axis analysis for the packing of glass ball with 600 μm diameter. In Fig. 4(d), warming color indicates narrow pore space and cooling color shows wide pore space. We can visually confirm the relation between real magnitude of void space and medial axis expression distinguished by different color. Table.3 shows porosity obtained by image processing technique at various glass ball diameter. All of the calculated porosity ranged from 34% to 38%, and exist in the packing pattern of tetragonal sphenoidal and cubical tetrahedral in a realistic packing condition. The frequency of effective pore and throat radii were shown in Fig. 5, and its peak value located almost at 70 μm~90 μm in pore radii and 60 μm ~ 70 μm in throat radii. The maximum pore radii attained to 270 μm correspond to the layer distance of tetragonal sphenoidal packing pattern. We confirm that 3DMA method can be applied for geometrical evaluation of porous media. The medial axis is affected by the flow channel, percolating backbone, and flow path in addition to other factors.

Table 2 Each packing system and geometrical data (refer to Mogami(1969))

| packing pattern | number of contact | layer distance | density | pore ratio | porosity(%) |
|-----------------------|-------------------|----------------|----------------------------|------------|-------------|
| simple cubic | 6 | 2R | ($\pi/6$) 0.5236 | 0.9098 | 47.64 |
| cubical tetrahedral | 8 | 2R | ($\pi/3\sqrt{3}$) 0.6046 | 0.6539 | 39.54 |
| tetragonal sphenoidal | 10 | $\sqrt{3}R$ | ($2\pi/9$) 0.6981 | 0.4324 | 30.19 |
| pyramidal | 12 | $\sqrt{2}R$ | ($\pi/3\sqrt{2}$) 0.7405 | 0.3504 | 25.95 |
| tetrahedral | 12 | $2\sqrt{2}/3R$ | ($\pi/3\sqrt{2}$) 0.7405 | 0.3504 | 25.95 |

070527 glass beads 0.6mm 3mmcube P=35.40%

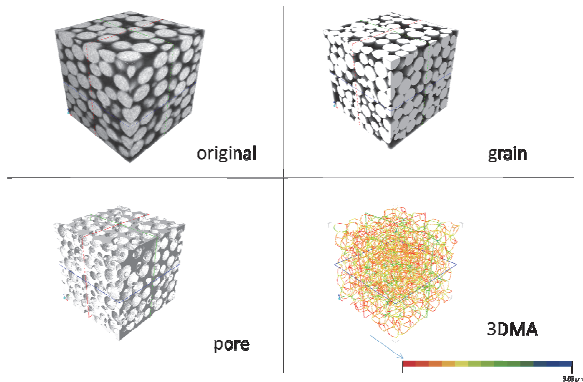


Fig. 4 Three Dimensional image of Medial Axis in glass beads with 600 μm diameter. (a) 3 dimensional original CT data. (b) 3 dimensional pore space image extracted from CT data. (c) grain distribution (d)3 dimensional medial axis image calculated from pore network data

Table 3 Glass ball diameter and porosity obtained with μ focus X-ray CT processing

| diameter of glass ball | porosity(%) |
|------------------------|-------------|
| 0.2mm | 36.74 |
| 0.4mm | 34.70 |
| 0.6mm | 35.40 |
| 0.8mm | 34.08 |
| 1mm | 36.58 |
| 2mm | 37.59 |
| 3mm | 37.35 |
| 4mm | 37.62 |

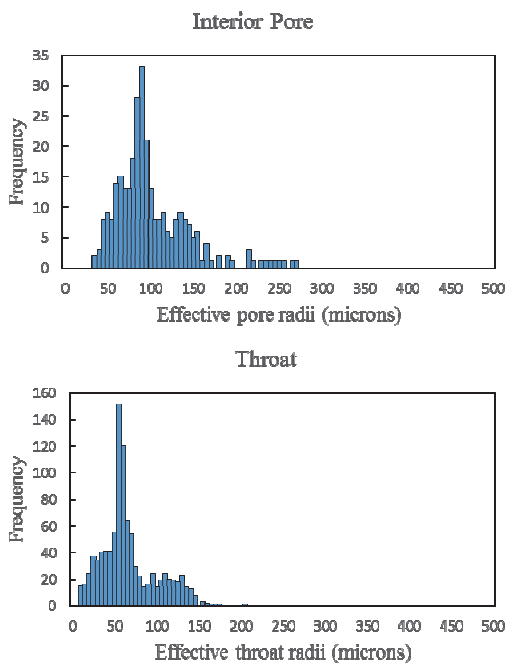


Fig. 5 Analyzed distribution of effective pore radii (a) and effective throat radii (b) for small glass ball

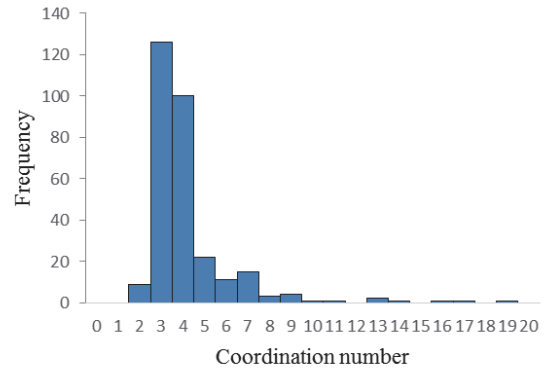


Fig. 6 Coordination number frequency of small glass ball aggregate

5. Geometrical and spatial information of small glass ball aggregate

Fig. 6 shows coordination number distribution. Coordination number means number of glass ball around a void space, namely show numerals of wideness on void space. In this glass ball aggregate coordination number distribute dominantly at 3 to 4 value. These values indicate almost regular packing condition and almost same glass ball size. Fig. 7 shows tortuosity distributions for X, Y and Z direction, respectively. Number of void space and connecting path at each face on analytical voxel are also shown for three perpendicular directions. Tortuosity distribution for three directions are almost same manner, but number of connecting path for different directions show small different value. Fig. 8 shows the shortest path distribution for three directions. In composite materials like a sandstone, the shortest path distributions show little bit different manner, this anisotropic spatial phenomenon is, in general, considered as main cause of anisotropic fluid flow of sedimentary rocks. Fig. 9 shows spatial distribution of each size of void space for different three perpendicular directions. Large void space scatter in the voxel, and can't form a route which flow a fluid. Network system with connecting void space are constructing under relatively complicated aggregate of various size of void space. Fig. 10 shows total volume of the shortest path for different directions. Total volume for all directions are almost same volume since glass ball has almost same diameter of 600 μm . We can analyze individual shortest path volume and summation volume of all path.

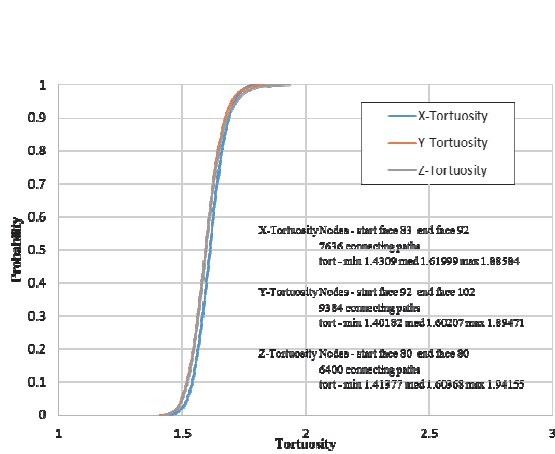


Fig.7 Tortuosity distribution for three perpendicular directions, and connecting path and number of void space information

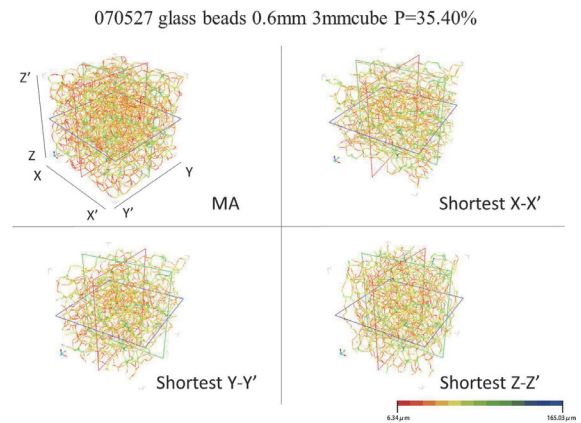


Fig.8 Whole medial axis distribution and the shortest path distribution for three perpendicular directions

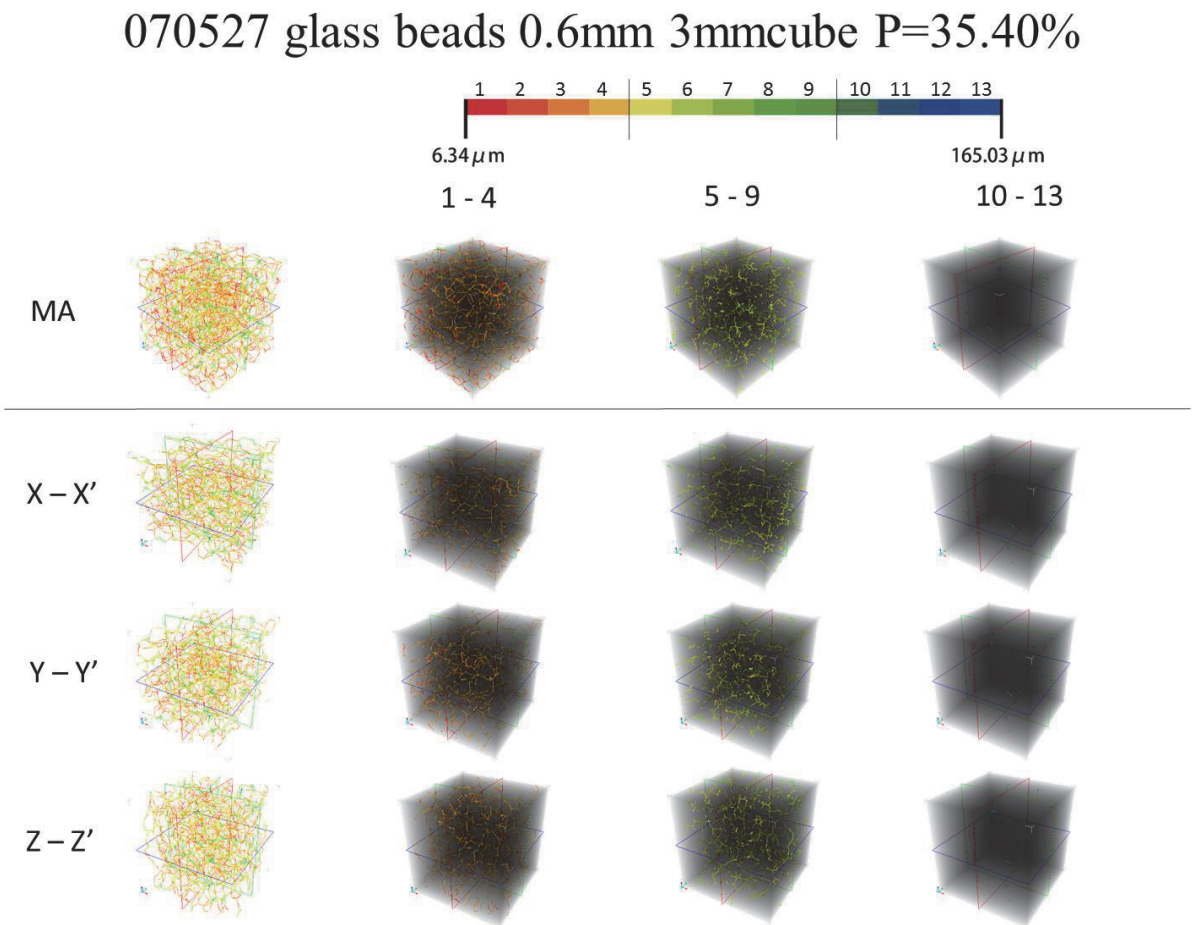


Fig. 9 Spatial distribution of void space for different category with different void radii

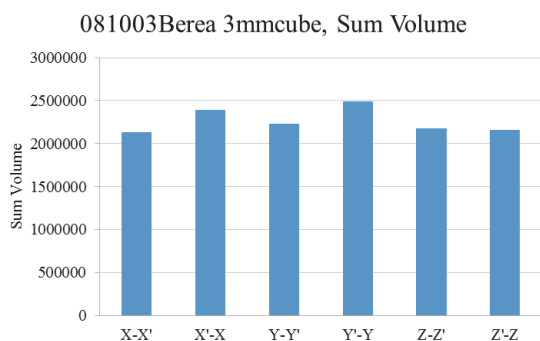


Fig. 10 Total volume distribution of the shortest path for different direction

6. Conclusion

To visualize the microstructure in small glass ball aggregate, micro focus X-ray CT system that can get three dimensional data simultaneously with high resolution of 10 micron is introduced. We analyzed three dimensional geometrical data of small glass ball aggregate obtained by micro focus X-ray CT. We introduced the three-dimensional medial axis (3DMA) method of Lindquist et al. (2000) to quantify the flow-relevant geometric properties of the voids structure in small glass ball aggregate. Using these data, we quantified the number of total pore, interior pore, throat, coordination number, connecting path between two faces, tortuosity and the shortest path distribution within an arbitrary region. It was found that the micro focus X-ray CT provides a useful geometrical and spatial information about individual particles, voids as a nondestructive visualizing tool.

References

- Coles, M.E., Hazlett, R.D., Spanne, P., Muegge, E.L. and Furr, M. J. (2002): Transport properties of porous media reconstructed from thin-sections, *SPE Journal*, 7(1), pp. 40-48.
- Hidajat, I., Rastogi, A., Singh, M. and Mohanty, K. K. (2002): Transport properties of porous media reconstructed from thin-sections, *SPE Journal*, 7(1), pp. 40-48.
- Hirono, T., Takahashi, M. and Nakashima, S. (2003): Direct imaging of fluid flow in fault-related rocks by X-ray CT, In Mees, F., Swennen, R., Van Geet, M. and Jacobs, P. (eds), *Applications of X-ray*

computed tomography in the geo-sciences, Geological Society, London, Special publications, 215, pp. 107-115.

- Karacan, C. O., Grader, A. S. and Halleck, P. M. (2003): Evaluation of local porosity changes in limestone samples under triaxial stress field by using X-ray computed tomography, In Mees, F., Swennen, R., Van Geet, M. and Jacobs, P. (eds), *Applications of X-ray computed tomography in the geo-sciences*, Geological Society, London, Special publications, 215, pp. 177-189.

Otani, J. and Obara, Y. (2003): X-ray CT for Geomaterials Soils, Concrete, Rock, Lisse : A.A. Balkema Publishers.

Verhelst, F., Vervoort, A., De Bosscher, Ph. and Marchal, G. (1995): X-ray computerized tomography, determination of heterogeneities in rock samples, In Proceedings of the 8th International congress on rock mechanics, Tokyo, Japan, September 25-30, pp. 105-108.

Vervoort, A., Wevers, M., Swennen, R., Roels, S., Van Geet, M. and Sellers, E. (2003): Recent advances of X-ray CT and its applications for rock material, In Otani, J. and Obara, Y. (eds), *X-ray CT for Geomaterials Soils, Concrete, Rocks*, pp. 79-91. Lisse : A.A. Balkema Publishers.

Lindquist, W. B., Venkatarangan, A., Dunsmuir, J. and Wong, T.F. (2000): Pore and throat size distributions measured from synchrotron X-ray tomographic images of Fontainebleau sandstones, *Journal of Geophysical Research*, Vol. 105, B9, pp. 21509-21527.

Lindquist, W. B. and Venkatarangan, A. (1999): Investigating 3D geometry of porous media from high resolution images, *Physics and Chemistry of the Earth Part A*, Vol. 25, No. 7, pp. 593-599.

Lindquist, W. B., Lee, S.M., Coker, D. A., Jones, K. W. and Spanne, P. (1996): Medial axis analysis of void structure in three-dimensional tomographic images of porous media, *Journal of Geophysical Research*, Vol. 101, B4, pp. 8297-8310.

Mogami, T. (1969): *Solid Mechanics*, Gihodo publication, pp. 904-914.

Takahashi, M., Takada, M., Sato, M. and Lin, W. (2014): Three Dimensional pore geometry and fluid flow of Kimachi sandstone under different stress condition: suggestion to conservation of tuffaceous world cultural heritage, *Engineering Geology for Society and Territory*, Proceedings of the 12th IAEG Congress, Vol. 8, 21, pp.135 – 138.